Fermilab Library
0 1160 0027350 2

STEWARD-1164

PREPRINTS

of the

STEWARD OBSERVATORY

THE UNIVERSITY OF ARIZONA
TUCSON, ARIZONA 85721 U.S.A.

No. 1164

ON THE RELEVANCE OF LINE-DRIVEN WINDS TO THE POST-MAXIMUM EVOLUTION OF CLASSICAL NOVAE

John C. Hayes

Department of Astronomy
University of Illinois, Urbana
and
Steward Observatory
University of Arizona

NOV 12 1993
LIBRARY

Illinois U., Urbana, Astronomy Dept.
Steward Observatory, Tucson

J Astrophys. J.

Submitted to The Astrophysical Journal.

Arizona Theoretical Astrophysics Preprint #93-52

ON THE RELEVANCE OF LINE-DRIVEN WINDS TO THE POST-MAXIMUM EVOLUTION OF CLASSICAL NOVAE

JOHN C. HAYES
Department of Astronomy, University of Illinois, Urbana
Steward Observatory, University of Arizona

Abstract

The standard thermonuclear runaway model for the classical nova outburst has had difficulty producing self-consistent, time-dependent models which evolve back to quiescence on timescales consistent with observations. This problem arose from the inability of these models to eject more than roughly 50% of the accreted material. Recent efforts to explore alternative mass-loss mechanisms have focused on energy deposition due to commmon envelope evolution. This paper explores an alternative mechanism: the input of radiative momentum due to the interaction of spectral lines with the velocity gradient in the expanding envelope. Rather than use the time-independent solutions for mass loss derived from the original work of Castor, Abbott, and Klein, this paper presents results from time-dependent simulations produced by incorporating the spectral line force term directly into the momentum equation solved by the hydrodynamics code. It is found that the effects of driving from spectral lines are secondary in comparison to the improved dynamical modeling which resulted from vastly improved numerical resolution of the envelope. As a result, it is now possible for numerical models to eject over 90% of their accreted envelopes, even when solar abundances are assumed. Difficulties remain with modeling the long-time behavior of these systems, however, due to limitations imposed by the use of a simple Lagrangean grid for the calculations.

Subject headings: stellar winds – stars: novae

1 INTRODUCTION

The aim of this paper is to explore an area of nova research which has long interested both theoreticians and observers, namely the timescale for classical novae (hereafter: CNe) to evolve from maximum light back to quiescence. This interest has been propelled by a long-standing inability of the standard thermonuclear runaway (TNR) model to produce nova simulations which evolve to quiescence on timescales consistent with observations. An enormous amount of theoretical work over the past two decades has helped to identify the basic mechanism of the classical nova outburst (that of a TNR at the base of an accreted envelope on a white dwarf), and to underscore the dependence of the outburst behavior upon such fundamental physical characteristics as the white dwarf mass and initial luminosity, the accretion rate, and the composition of the accreted envelope. Excellent reviews of the subject may be found in Truran (1990; 1982), Starrfield (1989a,b,c), Shara (1989), and Gallagher and Starrfield (1978). While such efforts as those by Starrfield, Truran, Sparks, and Kutter (1972), and Starrfield, Sparks, and Truran (hereafter: SST) (1974a,b; 1980; 1985; 1986) were successful in reproducing many of the gross features of the nova outburst with the TNR model, they found that in general their simulations were unable to eject more than roughly fifty percent of the accreted envelope (a notable exception being the extreme case of a simulated oxygen-neon-magnesium runaway described in SST (1986)). The implication of this behavior was that the remaining material would settle back onto the white dwarf and burn stably, thereby maintaining a high system luminosity for up to centuries (Truran 1982). Since most nova systems decline from maximum on timescales much less than this, it appeared that explosive mass ejection was insufficient to allow a nova system to return to quiescence on the proper timescale.

The problem of post-maximum mass loss was lessened somewhat by the eventual realization that the mean mass of nova progenitors should be roughly 1.2 $M_\odot$ (Ritter, Politano, Livio, and Webbink 1991; Truran and Livio 1986), rather than lying in the range from 0.5 to 1.0 $M_\odot$, which characterized the early studies. Nonetheless, even standard models at higher masses had difficulty in reproducing the long-term evolution of CNe, and the desire to find expedients to post-maximum mass loss remained. One such mechanism which has recently been studied quantitatively (Shankar 1990; Livio, Shankar, Burkert, and Truran 1990; Shankar, Livio, and Truran 1991), is the deposition of drag energy into the expanding nova envelope once it has exceeded the Roche dimension and encompassed the orbiting companion. These studies indicated that common envelope evolution appeared very promising both with regard to the timescale for mass loss and the effects on the morphology of the ejecta, provided that the assumptions of Bondi-Hoyle accretion and high efficiency of ejection (with regard to the effect of energy deposition) were valid.

A second mechanism of potential importance to nova evolution is the focus of this paper, namely, the effects of line-driven stellar winds on the expanding nova envelope. This paper will therefore discuss the degree to which the formalism initially developed by Castor, Abbott, and Klein (1975) (hereafter: CAK), and subsequently refined by Abbott (1980; 1982), and Pauldrach, Puls, and Kudritzki (1986), may be relevant to studies of novae. One may apply the CAK theory analytically using simple formulae which describe, for stars of early spectral type, the predicted steady rate of wind mass loss as a function of luminosity. A more general alternative is to drop the assumption of steady-state outflow and incorporate the CAK theory directly into a set of time-dependent hydrodynamic equations. Such an approach has been taken with calculations for O and Wolf-Rayet stars (e.g. Pauldrach *et.al* 1986), but no such incorporation into a time-dependent nova simulation has been published prior to this work. The work performed here parallels the work in Shankar (1990); i.e. Shankar considered the effects of common envelope evolution independent of line-driven winds, whereas this project takes the reverse approach.

The numerical calculations presented in this paper were performed with HYDRA, an implicit, 1-D, Lagrangean, radiation-hydrodynamics code. HYDRA is a heavily modified version of the code originally written by Kutter and Sparks (1972), and subsequently altered by SST (1980), and is consequently able to examine physical processes which are untreatable with the older code (traditionally referred to as NOVF). It is designed to take nova models which have been evolved through the accretion phase with NOVF and follow them through the subsequent outburst phase. This paper begins with a brief description of HYDRA, with emphasis on the main similarities and differences between it and NOVF. We then continue with

a very brief summary of the theory of spectral-line-driven stellar winds, and present a simple analytic application of this theory to nova evolution in Section 3. Section 4 presents the details of incorporating the CAK formalism into a time-dependent calculation, with a discussion of relevant physical and numerical concerns. The results of current numerical efforts are given in Section 5, followed by a summary and conclusions in Section 6.

2 A BRIEF DESCRIPTION OF HYDRA

HYDRA was developed as part of the thesis project of Hayes (1993), in an effort to study physical processes in nova evolution which are untreatable with NOVF. A number of differences between HYDRA and NOVF are worthy of mention:

(1) An algorithm for solving the hydrodynamic equations in the nonequilibrium, or two-temperature (2-T), diffusion approximation was added, allowing the code to perform radiation diffusion in either the standard or nonequilibrium prescription.

(2) The original matrix solver was replaced with standard routines from *Numerical Recipes* (Press, Flannery, Teukolsky, and Vetterling 1986), which were modified to improve computing speed. This change allows HYDRA to solve any system of equations which produce a block-diagonal matrix, unlike NOVF, which was "hard-wired" to solve a system of equations producing one particular set of non-zero matrix elements.

(3) The momentum equation (in both the 1- and 2-T prescriptions) now incorporates a term simulating the effects of spectral lines on the momentum balance in an expanding envelope.

(4) HYDRA contains an algorithm which repeatedly checks for and removes zones which are below 10^{-4} in optical depth, and which are simultaneously moving with velocities well in excess of the escape velocity and the local sound speed. Since such zones are no longer dynamically relevant, they are removed. This feature aids considerably in the computation of high-resolution models, such as those presented in Section 5.

(5) A set of routines were written to solve the radiative transfer equation, produce U, B, and V absolute magnitudes, and generate synthetic continua on the wavelength range from 10^{-8} to 10^{-2} cm.

The equations solved by HYDRA in the standard case of 1-T radiation diffusion are those of mass conservation, total momentum conservation, total energy conservation, energy transport, and the definition of velocity. The energy transport equation includes contributions from radiation and convection; the radiative portion is flux-limited. These equations are identical in form to those solved by NOVF, with the exception of the momentum equation, which contains the contribution from spectral lines coupled to the velocity gradient. In the event that radiation is allowed to propagate via 2-T diffusion, this set of equations is augmented by a relation governing the conservation of the total radiation energy density. In either case, the effects of spectral lines may be switched on or off, depending on the goals of the user.

In addition to the physics-related changes outlined above, many changes concerning I/O management, data storage, and coding logic (with the aim of improving performance on vector processors) were also made. Three portions of HYDRA, however, are direct carry-overs from NOVF. The first of these is the nuclear energy generation network, which is the same 13-element network used in all but the most recent incarnations of NOVF (which employ an expanded 80-element network). Secondly, the routines which read the equation of state and opacity tables into memory and those which handle the tabular interpolations at each grid point have also remained unchanged. Finally, the routines which handle the convective transport of energy and material employ the same physical prescriptions as those used in NOVF, although the energy transport routine was substantially reorganized to improve computing speed.

3 LINE-DRIVEN WINDS AND NOVAE

3.1 The Basic Picture of Line-Driven Winds

The central feature in the theory of line-driven stellar winds is the effect of atmospheric expansion upon the transfer of radiative momentum into the material. The presence of a strong velocity gradient in a stellar envelope will act to feed continuum flux into the core of a nearby spectral line, and thus absorption lines which might be saturated in a static atmosphere will intercept continuum flux which is orders of magnitude stronger than that available in the line core. The net result is an enhancement of the radiative momentum input to the material over what would naturally obtain in a static envelope. This mechanism is believed to be responsible for the observed mass loss rates of 10^{-6} $M_\odot$ yr^{-1} or more from O stars (Morton 1967b;

Lamers and Morton 1976). Theoretical efforts to understand the dynamical effects of spectral lines date back to Lucy and Solomon (1970). The single greatest advance in the theory came with the seminal work of CAK, noted previously in Section I. CAK developed an analytic theory which expresses the momentum input from spectral lines as a function of the velocity gradient and fitting constants which are computed by a stellar-atmospheres code; much of the improvement to the original CAK formulation has been manifested simply by revisions to the values of these fitting constants. CAK express the total force due to all lines as

$$f_{rad} = \frac{\sigma_e F}{c} M(t), \tag{1}$$

where σ_e is the electron-scattering opacity, and F is the total flux. The term $\sigma_e F/c$ is the total force due to continuous absorption; the function $M(t)$ is the so-called "force multiplier," which represents the effect of the line ensemble. CAK express $M(t)$ as

$$M(t) = kt^{-\alpha}, \tag{2}$$

where t is given by

$$t = \sigma_e \rho v_{th} \left| \frac{du}{dr} \right|^{-1}, \tag{3}$$

and k and α are the aforementioned fitting constants. In equation (3), v_{th} is the local mean ion thermal velocity.

In their original work, CAK found that the values of k and α which best fit the computed line force over the effective temperature range $30,000K \leq T_{\rm eff} \leq 50,000K$ were 1/30 and 0.7, respectively, assuming a solar composition. Since the publication of the CAK paper, work at improving the input physics used to compute the line force has been done by Abbott (1980;1982) and Pauldrach, Puls, and Kudritzki (1986). Abbott redid the earlier CAK work with atomic line data on all elements from H through Zn, while Pauldrach *et. al* modified the transfer equation to account for the variation of the angular size of the photosphere with height above the stellar surface. The net result of these studies was to revise the "best fit" value of k upward by an order of magnitude to 0.33, and to decrease the value of alpha by about 25%, to 0.53. Once the precise form of $M(t)$ is fixed, the expression for the total radiative force as given by equation (1) may be incorporated into the total momentum equation. CAK showed that an analytic solution to the momentum equation existed under the assumptions of spherically-symmetric, steady flow. Their resulting mass loss rate is

$$\dot{M} = \frac{4\pi GM}{\sigma_e v_{th}} \alpha (1-\alpha)^{\frac{1-\alpha}{\alpha}} (k\Gamma)^{\frac{1}{\alpha}} (1-\Gamma)^{\frac{\alpha-1}{\alpha}}, \tag{4}$$

which may be rewritten more simply (cf. Cassinelli 1979) as

$$\dot{M} = \frac{L}{v_{th} c} k^{\frac{1}{\alpha}} (1-\alpha)^{\frac{1}{\alpha}} \frac{\Gamma}{1-\Gamma}. \tag{5}$$

Here, Γ is the ratio of the total luminosity to the Eddington limit, given below by equation (7). Equation (5) predicts the rate of mass loss which will be experienced by a supergiant star with an effective temperature in the range $30,000K \leq T_{\rm eff} \leq 50,000K$, a given luminosity L, and the mean ion thermal velocity. The question of interest to which we turn next is what relevance, if any, that (5) has to the long-term evolution of CNe.

3.2 A Simple Application to Novae

Motivation for applying the CAK theory to novae may be obtained by considering the physical properties of a nova envelope near maximum light. A fast nova achieves a maximum visual luminosity on the order of 10^5 $L_\odot$, at which time the spectrum is characteristic of a supergiant of type F or earlier. The implication is then that these objects possess maximum luminosities, photospheric radii, and effective temperatures in or very near the range of parameter space covered by the CAK theory. A simple estimate of the effects of line-driven winds on nova evolution may be obtained in the following manner. First, we note that theoretical nova models typically possess, during the initial post-maximum phase of evolution, a roughly constant bolometric luminosity comparable to that given by the core mass-luminosity relation for AGB stars:

$$L_{\rm plat} \approx 6 \times 10^4 L_\odot (M_{\rm wd} - 0.5). \tag{6}$$

This value of the luminosity is frequently dubbed the "plateau luminosity" and is thus labeled with the "plat" subscript. This value of luminosity becomes comparable to the electron-scattering value for the Eddington limit,

$$L_{\rm edd} = 3.8 \times 10^4 L_\odot \left(\frac{M}{M_\odot}\right), \tag{7}$$

for white dwarfs with masses comparable to 1.2 $M_\odot$ or more. Thus if we write Γ as the ratio of $L_{\rm plat}$ to $L_{\rm edd}$ and evaluate v_{th} at an effective temperature of 10^4 K, we may rewrite (5) as

$$\dot{M}_{\rm wind} \approx 5.5 \times 10^{-7} \frac{L_{\rm plat}}{10^4 L_\odot} \frac{\Gamma}{1-\Gamma} \qquad (8)$$

If we know the initial mass of the accreted envelope, we may define and compute a wind depletion timescale as follows:

$$\tau_{\rm wind} = \frac{M_{\rm env}}{\dot{M}_{\rm wind}} \qquad (9)$$

Tables 1 and 2 present comparisons of the nuclear and wind depletion timescales for three different choices of white dwarf mass. All model sequences tabulated here are taken from the thesis work of Hayes (1993). In Table 1, all simulations were performed for accreted material of solar composition, whereas the sequences in Table 2 had CNO abundances a factor of 30 by mass over the solar value. One may see that even in this case, the most rapidly evolving model would require, by this simple analysis, several years to exhaust its available fuel through nuclear burning, whereas the assumption of mass loss rates derived from the CAK formalism aids enormously in reducing the timescale for envelope exhaustion/ejection. It is this simple fact which motivated the more sophisticated time-dependent treatment described below.

4 THE NUMERICAL APPROACH

While the results of the last section indeed appear encouraging, we must remain aware of the fact that the CAK formula for wind mass loss is computed for the time-independent flow of material with solar composition. Furthermore, the value of the force multiplier depends upon constants which have been optimized for effective temperatures in a fairly narrow range. While the revised values of k and α appear to be applicable over a fairly broad range of temperature and density (see Abbott 1980; 1982 or Pauldrach *et. al* 1986), the fact remains that $\dot{M}_{\rm wind}$ as derived by CAK assumes time-independent flow. A better approach to applying the CAK formalism is to drop the derived expression for $\dot{M}_{\rm wind}$ and incorporate the line force directly into the time-dependent momentum equation solved by a hydrodynamics code.

4.1 Physical Concerns

The formulation of the line-force term described above was designed for use in supergiants primarily of spectral types O and B. We have seen that novae at maximum bear some superficial resemblance to early-type supergiants, but we must note the physical differences between these classes of objects and estimate the consequences of these differences. One difference is the structure of the objects themselves. O stars may be considered in the first approximation to be essentially static below the photosphere; the large transsonic outflows, while ultimately being fed by material from below, are dominant in the outer, optically thin regions of the stellar envelope. Fast CNe, by contrast, experience an initial outflow that originates well below the photospheric depth. This outflow is sometimes referred to as an "optically-thick wind" in time-independent analyses (e.g. Ruggles and Bath 1979; Kato 1983, 1985; Kato and Hachisu 1988, 1989), or privately as "burst ejection" by other researchers. What we may expect is that the effects of line-driving will become increasingly dominant once the initial phase of explosive ejection has passed. This major difference, between O stars and novae, in the initial conditions at the onset of line-driven outflow provides the basic motive for incorporating the line-force directly into the hydrodynamic equations, rather than relying upon the analytic solution for $\dot{M}_{\rm wind}$.

In addition to differences in the initial conditions leading to mass outflow, structural differences between O stars and novae lead to greatly differing values of the surface gravity. However, Abbott (1982) has found that the computed line acceleration is not strongly sensitive to $\log(g)$. Thus this difference should not be of great concern here.

Of potentially greater significance to nova modeling is the dependence of the computed line force upon the composition of the envelope. The original values of k and α chosen by CAK were computed for material of solar composition; we know from observational studies that CNe (particularly fast CNe) are frequently enriched in heavy elements. Indeed, total Z mass fractions of 0.6 or more are commonly reported in observational studies of the faster CNe (e.g. Lance, McCall, and Uomoto 1988; Snijders *et. al* 1987; Stickland *et. al* 1981). The original CAK work and the subsequent studies by Abbott indicated a dependence of the line force upon Z of the following

form:

$$a_l \propto Z^{1-\alpha} \tag{10}$$

The dependence is less than linear because once a line becomes optically thick, increasing the opacity in that line cannot increase the resulting acceleration. Thus a choice of 0.53 for α (which was that used for all studies discussed here) leads to a roughly $Z^{1/2}$ dependence of a_l upon α. In spite of this relatively soft relation between a_l and α, Abbott found that the mass loss rate scaled almost linearly with Z; his expression is

$$\begin{aligned} \dot{M}(M_\odot \text{ yr}^{-1}) &= 1.4 \times 10^{-15} \frac{(L/L_\odot)^{1.98}}{(M(1-\Gamma)/M_\odot)^{1.03}} \\ &\times \frac{(Z/Z_\odot)^{0.94}}{(T_{\text{eff}}/10^4 K)^{0.02}} \end{aligned} \tag{11}$$

which is valid for T_{eff} between 10,000 and 50,000 K. Of notable interest here is the extremely weak dependence upon T_{eff} within that specified range. In any case, trial nova sequences computed with the line force term adopted a $Z^{0.94}$ dependence for the value of k, the line force proportionality constant. This was done to estimate the maximum conceivable effect that line driving might have upon the nova wind. This dependence was retained for the results presented in Section 5, even though such a dependence of a_l upon Z is probably unphysically large. We shall see, however, that even models with such extreme levels of line-driving do not eject substantially greater amounts of material than that ejected by the corresponding models without line-driving effects. This will help to reinforce our eventual conclusion that line-driving is *not* a dominant effect in nova evolution with regard to envelope exhaustion.

4.2 Numerical Concerns: The Need for Better Envelope Resolution

A major impediment to the first efforts at incorporating the CAK formalism into a nova simulation was the presence of large post-maximum oscillations in both the bolometric and visual lightcurves, as illustrated by Figures 1 and 2. Obviously these oscillations are neither smooth nor regular, but instead appear indicative of errors in the solution for the emergent luminosity. The oscillations at long times, particularly for the visual luminosity, are so large that it is difficult to make any statement about the long-term evolution of the lightcurve. The culprit behind this problem is the remarkably small number of zones in the white dwarf model used to define the accreted envelope. To understand how such a situation may arise, we must review how the pre-outburst accreting phase is treated by NOVF (cf. SST 1980). All white dwarf models produced by this code are spanned by 96 mesh points running from the stellar core to the surface; thus the entire white dwarf is divided into 95 zones. Accretion is simulated by starting with the surface zone and changing the composition within that zone and the total stellar mass consistent with the assumed accretion rate and composition of the accreted material. Once the total accreted mass equals the mass of the surface zone (at which point the composition of that zone is identical to the composition of the accreting material), the process is repeated with the zone immediately interior. Eventually the total mass of the accreted envelope becomes great enough to initiate a TNR, at which point the subsequent dynamic evolution is limited to the zones which define the accreted envelope. In the model displayed in Figures 1 and 2, there were 14 zones within the accreted envelope. Given that the dynamic events comprising the nova outburst are confined to the accreted envelope itself, we see that we are effectively computing a 14-zone simulation of a hydrodynamic event. To appreciate the significance of this from a physical standpoint, remember that the equations of total momentum conservation and energy transport contain gradient terms which specify the spatial variation of pressure (in the case of momentum conservation) and temperature (in the case of energy transport). Thus we see that good spatial resolution of the envelope is crucial to assure the correct momentum balance in the radiating fluid and the correct level of radiative energy transport. At outburst maximum, this model sequence spanned, between the nuclear burning shell and the envelope surface, 8 decades in velocity, 16 decades in density, 4 decades in temperature, 5 decades in radius, and 18 decades in pressure. To expect such a physical environment to be adequately described by 14 grid points is clearly unrealistic.

Because of the clear need for improved numerical resolution of the nova envelope, the very first efforts in this project were directed toward developing an algorithm which would take a 95-zone white dwarf model and reinterpolate the accreted envelope onto a new grid with a much larger number of zones. The original 95-zone models are gridded such that the ratio of adjacent zone masses is a constant. The rezoning al-

gorithm developed for this project allows the original 95-zone model to be regridded between the original surface gridpoint and any desired interior grid point. Additionally, the user may specify the new ratio of zone masses in the regridded portion. Adjusting this ratio has the effect of shifting the location (with respect to mass) of the gridpoints inward or outward. In the numerical results tabulated below, 95-zone models are labeled as "low-resolution" runs, and regridded models are labeled as "high-resolution" runs. All high-resolution models are envelope models which contain 295 zones between the surface grid point and the core-envelope interface (CEI), and 5 of the original white dwarf core zones beneath the interface. The original zoning of the white dwarf is sufficiently coarse so that the five zones below the CEI contain at least as much mass as the 295 zones above it. The bulk of a nova outburst typically proceeds on timescales very short compared to the time for significant heat conduction into the white dwarf core, but the rezoning prescription given here retains some of the envelope's ability to communicate thermally with the underlying white dwarf.

Once the high-resolution model is constructed, it is input to HYDRA, and the subsequent evolution to, through, and past outburst maximum is followed. One point of interest that should be noted here concerns energy conservation. The rezoning algorithm computes the total integrated energy both before and after rezoning. The difference between the two numbers is divided by the original energy and typed out as a relative energy conservation error. A typical value for this number is 10^{-10}. The reason that this number is so low is that the rezoning is performed before the envelope becomes dynamic; thus the profiles of the relevant physical variables are still relatively flat. This point about energy conservation is made here so that the reader will understand that the fairly spectacular differences in mass loss between the low- and high-resolution sequences shown below are not due to spurious errors in the total energy content. In addition, the rezoning was performed at different points in time prior to runaway to verify that rezoning did not distort other physical properties of the pre-outburst model. Models which were rezoned immediately after the accreted envelope had become fully convective (when the energy generation rate was still several orders of magnitude below its eventual maximum), yielded precisely the same results as those which were rezoned much earlier, before convection had become dominant. Thus it was clear that the rezoning process had not introduced artificial effects influencing the outburst behavior.

5 RESULTS

5.1 Resolution Effects

To explore the effects of numerical resolution upon a nova simulation, we will consider again the array of model sequences first discussed in Section III. We have a total of six model sequences encompassing three choices of the white dwarf mass (1.0, 1.25, and 1.35 $M_\odot$) and two choices of heavy element composition (Z = 0.02 and 0.60) for each mass. In all runs with a Z of 0.02, the abundance distribution among the Z elements was solar. In the runs with a Z of 0.60, the nitrogen abundance was solar, but the C/O ratio was 2:1 (by mass) for the 1.0 and 1.25 $M_\odot$ white dwarfs and 1:2 for the 1.35 $M_\odot$ white dwarf sequences. Nitrogen was held at its solar value because the primary goal of the varying the composition was to delineate the effects of carbon and oxygen upon the outburst strength. The C/O abundance ratio was reversed for the 1.35 $M_\odot$ because (1) we expect that abundance enhancements in the accreted envelope arise from mixing between the envelope and the underlying white dwarf, rather than from enrichments in the donor star, and (2) a 1.35 $M_\odot$ white dwarf is more likely to be composed primarily of oxygen, neon, and magnesium rather than carbon and oxygen. The mass accretion rate was 10^{-9} $M_\odot$ yr^{-1} in all cases. The initial white dwarf luminosity was 0.005 $L_\odot$ for the 1.0 $M_\odot$ and 1.25 $M_\odot$ sequences (models 1-6) and 0.006 $L_\odot$ for the 1.35 $M_\odot$ sequences (models 7-9). This difference arose from limitations upon the equation of state tables encountered with 1.35 $M_\odot$ white dwarfs when the luminosity was at lower values.

We will begin our quantitative comparison of high- and low-resolution nova simulations by examining the effects of zoning upon the computed lightcurves. Tables 3 and 4 list the maximum bolometric and visual magnitudes achieved for six model sequences computed with both low- and high-resolution envelopes. All low-resolution runs were full white dwarf models with 95 zones comprising the white dwarf plus accreted envelope. The number of zones in the accreted envelope varied with each model, but ranged from a low of 14 (in the run with M = 1.25 $M_\odot$, Z = 0.6) to a high of 38 (in the run with M = 1.35 $M_\odot$, Z = 0.02). In all high-resolution runs, the accreted enve-

lope was spanned by 295 zones between the surface and the base of the burning shell; an additional five "core" zones below the burning shell were retained.

Accompanying the tabular data are plots (Figures 3 through 6) which display the bolometric and visual lightcurves in the case of low- and high-resolution for a representative sample of model sequences. These plots only cover a brief period of post-maximum evolution so that the some of the main features listed below can be seen easily. Long-time plots which better display the turn-off timescale are presented in Section 5.3. Noteworthy features of these Figures 3-6 and Tables 3 and 4 include the following:

(1) Peak bolometric luminosities are systematically higher in the high-resolution runs than in their low-resolution counterparts, although the difference tends to be small (the exception being the 1.0 $M_\odot$ white dwarf with the high-CNO envelope).

(2) Peak visual luminosities are significantly higher for 300-zone nova envelopes.

(3) The low-resolution runs are characterized, for the models with high-CNO envelopes, by large and erratic post-maximum fluctuations in the bolometric and visual lightcurves. These fluctuations are greatly reduced in the corresponding 300-zone runs.

(4) The high-resolution 1.0 $M_\odot$ run with $Z = 0.02$ displays a pronounced post-maximum dip in the visual lightcurve. This feature, which is present to some degree in most of the model sequences, is missed entirely by the low-resolution runs.

The trends noted above may be understood on the basis of simple physical principles. The peak visual luminosities are more susceptible to effects of zoning than the peak bolometric luminosities because the computed visual maximum depends upon the effective temperature, which in turn depends on the computed optical depth scale. An expanding envelope with a surface radius greater than 10^{12} cm and which is spanned by only a dozen or so gridpoints will be terribly underresolved with regard to optical depth, particularly once a significant portion of the envelope has become optically thin. The large post-maximum fluctuations in the lightcurves of the low-resolution models are also easily understood as artifacts of underresolved optical depth scales (critical for fixing the effective temperature and evaluating the surface boundary condition on luminosity) and temperature gradients (required for the solution of the transport equation). The last feature noted in the list above also illustrates the danger of underresolving the envelope. The post-maximum dip in the visual lightcurves, which is most prominent in models with solar or mildly CNO-enhanced envelopes, is an effect of the changing bolometric correction as the envelope expands. The envelope is initially in a state of small radius and high effective temperature. As the envelope begins to expand, T_{eff} drops, causing progressively more radiation to be produced in the optical portion of the spectrum. As the photospheric radius increases, the wavelength of maximum emission continues to redden, and the visual luminosity reaches a maximum and begins to decline. At some point, however, the envelope begins to become optically thin, which causes the photosphere to retreat and thus reverses the decline in visual luminosity. The visual luminosity reaches a secondary maximum and begins to decline again, albeit much more slowly this time because now the mass loss has entered a phase of near steady-flow conditions. This type of behavior is missed entirely by the low-resolution models, which are simply unable to resolve the optical depth scale adequately.

Having established the importance of adequate envelope resolution to the computation of bolometric and visual lightcurves, let us now examine the effects of zoning upon the dynamics of the expansion itself. We begin by noting the effects of zoning on the maximum energy generation rate. In five of the six model sequences considered, the maximum energy generation rate was higher in the 300-zone runs than in their 95-zone counterparts. The exact numbers for all sequences are provided in Tables 5 and 6. Of greatest relevance to the discussion in this chapter, however, are the numbers presented in Table 7, in which we see the effects of envelope resolution upon mass ejection. Given for each model sequence, for both high- and low-resolution cases, is the fraction of the accreted envelope which had been ejected by the end of the run. It must be emphasized that the end of the run does not always correspond to the time at which no further interesting evolution takes place. The point at which the high-CNO runs were terminated was determined by HYDRA's ability to continue following the evolution. Low-resolution runs are particularly susceptible to large errors once the envelope has become greatly distended; these errors inevitably swamp the solution and prevent further calculation. This is responsible for the seemingly peculiar variation of mass ejection with composition, most visible in the 95-zone models.

The high-CNO runs, which produce the most violent outbursts and which would thus be expected to ultimately eject the most mass, show less fractional mass ejection because these runs become numerically unstable sooner than less violent sequences. Better envelope resolution and increased outburst violence have competing influences on HYDRA's ability to track the model's evolution into the post-maximum phase. The mass fractions quoted in Table 7 are therefore lower limits determined in part by the numerical longevity of the model.

The most obvious feature of Table 7 is not the variation of mass ejection with envelope composition, but rather the remarkable difference with regard to mass ejection between the low- and high-resolution runs at *any* white dwarf mass or composition. We can see that when the expanding envelope is well resolved, even models with solar composition are able to eject at least 80 to 90 percent of their accreted envelopes without the aid of spectral lines or any other mass-loss enhancement. The implication of this is that TNR-induced mass ejection is far better at removing the nova envelope than previously supposed. Thus even without considering the effects of mass-loss enhancement by line-driving or common envelope evolution, some of the traditional wisdom regarding the dependence of mass loss upon chemical composition must be re-examined. The primary influence of composition in these new runs is upon the timescale for mass ejection, rather than the actual amount of ejected mass. For example, the 1.0 $M_\odot$, solar composition, 300-zone model sequence had ejected 88% (5.6×10^{-5} $M_\odot$ out of 6.4×10^{-5} $M_\odot$ initially accreted) of its envelope after 1530 days of evolution, whereas the 1.0 $M_\odot$ model with Z = 0.6 ejected 79% percent (1.7×10^{-5} $M_\odot$ out of an initial 2.1×10^{-5} $M_\odot$) of its envelope after only 30 days. Similarly, the 1.25 $M_\odot$ model with solar composition ejected 91% (1.9×10^{-5} $M_\odot$ out of an initial 2.1×10^{-5} $M_\odot$) of its envelope over 700 days of evolution, while the corresponding run at Z = 0.6 ejected 93% (7.1×10^{-6} $M_\odot$ out of 7.6×10^{-6} $M_\odot$) in only 15 days. These figures correspond to average mass-loss rates of order 10^{-5} $M_\odot$ yr^{-1} in the case of solar envelopes and 10^{-4} $M_\odot$ yr^{-1} in the case of envelopes with Z = 0.6. These mass-loss rates are beyond anything obtainable with spectral line-driving in most cases, but we must remember that this mass loss corresponds to explosive shell ejection and is likely not appropriate for consideration in a "wind" context. Figures 7 and 8 show the actual behavior of the mass loss with time for these two sequences. Shown is the fractional amount of mass ejected vs. time; the zero point of time is the same as that for the corresponding lightcurves. One may clearly see that the mass loss rate is by no means constant, but rather is characterized by a substantial level of prompt ejection which then tapers off to a much lower rate.

5.2 The Effect of Spectral Lines on Mass Loss

Given the degree of mass loss enhancement obtainable through improved resolution of the envelope, one may wonder how great an effect line-driving may have on the system. Table 8 presents the results of nova simulations with line-driven winds for all 3 white dwarf masses and two choices of composition. All model sequences computed used 300-zone envelope models. In the runs with solar composition, values of 0.33 and 0.53 were used for k and α, respectively. In the runs with Z = 0.6, α was held at 0.53, but k was boosted by a factor of $(0.6/0.02)^{0.94} = 24.5$ to a value of 8.1. Recall that this is likely an unphysically large increase due to composition effects alone, but that fact will not damage the arguments given below.

Examination of the results in Table 8 reveals the striking inability of line-driving to enhance the loss of mass significantly beyond that achieved by the models without line-driving. Of course, one must acknowledge that a model which ejects 90% of its accreted envelope *without* the aid of line-driving leaves little room for substantial increases in the total mass ejected, although line-driving may considerably influence the velocity structure of the outflow. In all runs presented in Table 8, the models were evolved until the zones which had not escaped had begun falling back toward the white dwarf. The accuracy of the computation at that point may be called into question, however, for the following reason: by the time a model sequence reaches the point where it is unable to eject any more mass, all but 10 or 20 zones have become highly supersonic, highly in excess of escape velocity, and extremely optically thin. In other words, such models only have about 10 or 20 zones which are dynamically relevant and which span the region from the white dwarf surface past the photosphere (which is still at a radius of roughly 10^{12} cm). Thus even the 300-zone models eventually reach a state which is analogous to that held by the low-resolution models from the beginning. The implication is that one needs adaptive grid techniques to follow the evolution of the line-driven wind at late times. It may be that

with such techniques, one could follow the evolution of the system (with or without line driving) until all of the accreted mass was removed from the white dwarf. This question, unfortunately, is beyond the scope of this paper.

5.3 The Post-Maximum Visual Decline

The resolution problems encountered at late times in a numerical simulation are consequences of using a Lagrangean grid in HYDRA. Since the grid points remained fixed in the fluid, substantial expansion will inevitably lead to a situation in which the physical domain of interest is spanned by an insufficient number of grid points. Because the CNO-enriched simulations typically produce the most violent explosions, these model sequences are the most difficult to evolve for long periods of time. Furthermore, since line-driven winds enhance the envelope expansion even further, problems with late-time envelope resolution become even more severe when such effects are included. While it is possible to produce long-timescale lightcurves for nova simulations of solar or mildly CNO-enriched abundances, even when line-driven winds are included, the high-CNO runs are extremely difficult to maintain for evolution times long enough to watch the system return to pre-outburst luminosities. The best-behaved simulation with high CNO enhancements produced by HYDRA to date is a 500-zone simulation for a 1.25 $M_\odot$ model corresponding to model 6 in Tables 3-7. The lightcurve for this sequence, in which line-driving effects were *not* included, is given in Figure 11. Accompanying this plot are those given in Figures 9 and 10, which show long-time evolution for model sequences with envelopes of solar composition, with and without line-driven winds. In Figure 9 the white dwarf mass is 1.0 $M_\odot$, whereas in Figure 10 the mass is 1.25 $M_\odot$. The chief effect of line-driving in these runs is the dispersal of the envelope above the photosphere; because the initial explosion is so efficient at accelerating the bulk of the envelope past escape velocity, the line-driven winds act primarily as an "afterburner," accelerating material which is no longer bound to the system. In all runs performed thus far, the spectral line acceleration eventually becomes significant in regions which have not yet escaped, but this consistently occurs near the time when the grid has become so extended that further evolution can not be followed. Therefore, because of the limitations of a simple Lagrangean grid, the phase of nova evolution where CAK-style winds might be a dominant influence is not currently accessible with these simulations. However, we have already seen that the nova simulations given here have already ejected the vast majority of their accreted material; thus the extreme late-time effects of line-driven winds should be of secondary importance in expediting a nova's return to quiescence.

Of all the model sequences presented in this papers, the best quantitative estimate of the long-time behavior of a fast nova model is provided by the simulation displayed in Figure 11. This sequence was produced by a 500-zone version of model 6, and was computed as part of an effort to determine whether even higher degrees of envelope resolution could allay late-time numerical problems significantly. That this sequence is well on its way to quiescence, without the aid of line-driving or other special mechanisms, is immediately apparent. One may also see the effects of late-time resolution manifesting themselves after about day 40 in the outburst, but the general behavior is consistent with expectations. It is also worth noting the presence of a sub-maximum in the visual luminosity which precedes the main maximum. This feature, which is entirely an effect of the temporal behavior of the effective temperature as noted previously, bears some resemblance to the "pre-maximum halt" observed in some nova systems (McLaughlin 1942). In spite of the positive features of this model, we must remain aware of other basic processes, apart from the effects of line-driven winds, which are ignored in this calculation. Recall that all simulations presented herein neglect common-envelope evolution entirely. In addition, the potentially important effects of revised heavy-element opacities (Rogers and Iglesias 1992; Seaton, Yan, Mihalas, and Pradhan 1993), as noted by Kato and Iben (1992), have been neglected in this work. However, these omissions may all be overshadowed by the assumption of spherical symmetry, which has characterized all theoretical simulations of nova lightcurves to date. Since we picture the decline of the visual lightcurve as the result of photospheric retreat into progressively hotter regions of the envelope, such behavior should be strongly dependent upon the geometry of the envelope itself. Observations of recent novae such as Nova Cyg 1992 (e.g. Hauschildt *et. al* and references therein) and many of the older novae (see Mclaughlin 1960 for a classic review) indicate that spherical symmetry may be a poor approximation to the truth, even at relative early stages in the outburst. Because of this,

the predictive power of one-dimensional simulations at any level of sophistication is likely to be very general; detailed insight into the post-maximum behavior of these objects will most likely depend strongly on geometric effects hitherto ignored in theoretical work (notable exceptions being that of Livio *et. al* 1990 and Shankar *et. al* 1991).

6 SUMMARY AND CONCLUSIONS

This paper began by presenting what was regarded as a long-standing problem with the standard TNR model of a nova outburst: the timescale for the return to quiescence. We have seen that much of this problem was due to hydrodynamic errors resulting from inadequate envelope resolution. The dynamics of the expanding envelope and the details of energy transport demand that gradients in temperature, pressure, and optical depth be resolved properly. We have seen that enormous improvements are obtainable with the use of a simple Lagrangean grid with an appropriate number of zones, but we have also seen that such techniques inevitably become inadequate during the post-maximum evolution. Because of limitations imposed by the use of a Lagrangean grid in the numerical simulations, the late-time evolution of these models is extremely difficult, and in many cases impossible, to follow. Improvements to the time-dependent, one-dimensional modeling of classical novae will demand more sophisticated gridding algorithms employed thus far. The main result of these 1-D simulations is to show that the effects of line-driven stellar winds are secondary in comparison to the effects of the TNR itself, although we must remember that detailed estimates of late-time lightcurve evolution are likely to demand knowledge of multi-dimensional effects ignored in these and all 1-D studies.

The author gratefully acknowledges useful discussions with and assistance from Dimitri Mihalas, who provided invaluable counsel during the developement of HYDRA, as well as financial support. The author would also like to thank Jim Truran for years of stimulating discussions of novae and for additional financial support. Additionally, the author would like to thank Sumner Starrfield for providing access to the original nova code from which HYDRA was derived. This work was supported in part by the University of Illinois, by NSF grants AST 92-17969 and AST 93-96039 at the University of Chicago, and by NASA grant NAGW-2421 at the University of Illinois. The computer simulations presented here were performed at the National Center for Supercomputing Applications at the University of Illinois.

REFERENCES

Abbott, D.C. 1980, *Ap. J.*, **242**, 1183.

Abbott, D.C. 1982, *Ap. J.*, **259**, 282.

Cassinelli, J. P. 1979, *Ann. Rev. Astron. Astrophys.*, **17**, 275.

Castor, J.I., Abbott, D.C., and Klein, R.I. 1975, *Ap. J.*, **195**, 157.

Ensman, L. M. 1990, Thesis (University of California at Santa Cruz).

Gallagher, J. S. and Starrfield, S. 1978, *Ann. Rev. Astr. Ap.*, **16**, 171.

Hauschildt, P. H., Starrfield, S., Austin, S., Wagner, R. M., Shore, S. N., and Sonneborn, G. 1993, *Ap. J.*, in press.

Hayes, J. C. 1993, Thesis (University of Illinois).

Kato, M. 1983, *Pub. Astron. Soc. Japan*, **35**, 507.

— 1985, *Pub. Astron. Soc. Japan*, **37**, 19.

Kato, M. and Hachisu, I. 1988, *Ap. J.*, **329**, 808.

—1989, *Ap. J.*, **346**, 424.

Kutter, G. S. and Sparks, W. M., 1972, *Ap. J.*, **175**, 407.

Lamers, H.J.G.L.M., and Morton, D. 1976, *Ap. J. Suppl.*, **32**, 715.

Lance, C. M., McCall, M. M., and Uomoto, A. K. 1988 *Ap. J. Suppl.*, **66**, 151.

Livio, M., Shankar, A., Burkert, A., Truran, J.W. 1990, *Ap. J.*, **356**, 250.

McLaughlin, D. B. 1942 *Pop. Astr.*, **50**, 233.

— 1960 in *Stars and Stellar Systems VI: Stellar Atmospheres*, ed. J. Greenstein, (Chicago: University of Chicago Press), p. 585.

Morton, D. 1967a, *Ap. J.*, **147**, 1017.

— 1967b, *Ap. J.*, **150**, 535.

Press, W. H., Flannery, B. A., Teukolsky, S. A., Vetterling, W. T. 1986, *Numerical Recipes*, (Cambridge: Cambridge University Press).

Ritter, H. Politano, M., Livio, M., and Webbink, R. F. 1991, *Ap. J.*, **376**, 177.

Rogers, F. J., and Iglesias, C. A. 1992, *Ap. J. Suppl.*, **79**, 507.

Ruggles, C., and Bath, G. T. 1979, *Astr. Ap.*, **80**, 97.

Seaton, M. J., Yan, Y., Mihalas, D. M., and Pradhan, A. K. 1993, *M. N. R. A. S.*, submitted.

Shankar, A. 1990, Thesis (University of Illinois).

Shankar, A., Livio, M., Truran, J.W. 1991, *Ap. J.*, **374**, 623.

Shara, M. M. 1989, *PASP*, **101**, 5.

Snijders, M. A. J., Batt, T. J., Roche, P. F., Seaton, M. J., Morton, D. C., Spoelstra, T. A. T., and Blades, J. C. 1987, *M.N.R.A.S*, **228**, 329.

Starrfield, S. 1988*a*, in *Multi-Wavelength Astrophysics*, ed. F. Córdova, (Cambridge: Cambridge University Press).

— 1989*b*, in *Classical Novae*, eds. Bode and Evans, (New York: Wiley).

— 1989*c*, in *Proceedings of IAU Colloquium No. 122, Physics of Classical Novae*, ed. A. Cassatella (Berlin: Springer).

Starrfield, S., Sparks, W. M., and Truran, J. W. 1974*a*, *Ap. J. Suppl.*, **28**, 47.

— 1974*b*, *Ap. J.*, **192**, 647.

Starrfield, S., Sparks, W. M., and Truran, J. W. 1980, *Ap. J.*, **239**, 988.

Starrfield, S., Sparks, W. M., and Truran, J. W. 1985, *Ap. J.*, **291**, 136.

Starrfield, S., Sparks, W. M., and Truran, J. W. 1986, *Ap. J. Lett.*, **303**, L5.

Starrfield, S., Truran, J. W., Sparks, W. M., and Kutter, G. S. 1972,*Ap. J.*, **176**, 169.

Stickland, D. J., Penn, C. J., Seaton, M. J., Snijders, M. A. J., and Storey, P. J. 1981, *M.N.R.A.S.*, **197**, 107.

Truran, J.W. 1982, in *Essays in Nuclear Astrophysics*, eds. C.A. Barnes, D.D. Clayton, and D.N. Schramm, (Cambridge: Cambridge University Press), p. 467.

Truran, J. W. 1990, in *The Physics of Classical Novae*, eds. A. Cassetella and R. Viotti (Heidelberg: Springer-Verlag), p. 373.

Truran, J. W., and Livio, M. 1986, *Ap. J.*, **308**, 721.

Figure Captions

Figure 1: Bolometric lightcurves for a nova simulation with 95 zones in the numerical grid, 14 of which lay in the accreted envelope. The white dwarf mass is 1.25 $M_\odot$, and Z = 0.6 in the accreted envelope.

Figure 2: Visual lightcurves for a nova simulation with 95 zones in the numerical grid, 14 of which lay in the accreted envelope. The white dwarf mass is 1.25 $M_\odot$, and Z = 0.6 in the accreted envelope.

Figure 3: Low and high resolution bolometric lightcurves for a 1.0 $M_\odot$ with an envelope of solar composition.

Figure 4: Visual lightcurves for the model sequences in Figure 2.

Figure 5: Low and high resolution bolometric lightcurves for a 1.25 $M_\odot$ with Z = 0.6 in the envelope.

Figure 6: Visual lightcurves for the model sequences in Figure 4.

Figure 7: The fractional mass ejected as a function of time for the high resolution model sequence with a solar envelope on a 1.25 $M_\odot$ white dwarf.

Figure 8: The fractional mass ejected as a function of time for the high resolution sequence with a CNO-enriched (Z =0.6) envelope on a 1.25 $M_\odot$ white dwarf.

Figure 9: The visual lightcurve for a solar-composition envelope on a 1.0 $M_\odot$ white dwarf with line-driving included.

Figure 10: The visual lightcurve for a solar-composition envelope on a 1.25 $M_\odot$ white dwarf with line-driving included.

Figure 11: The visual lightcurve for a CNO-rich envelope on a 1.25 $M_\odot$ white dwarf with line-driving excluded.

FIGURE 1

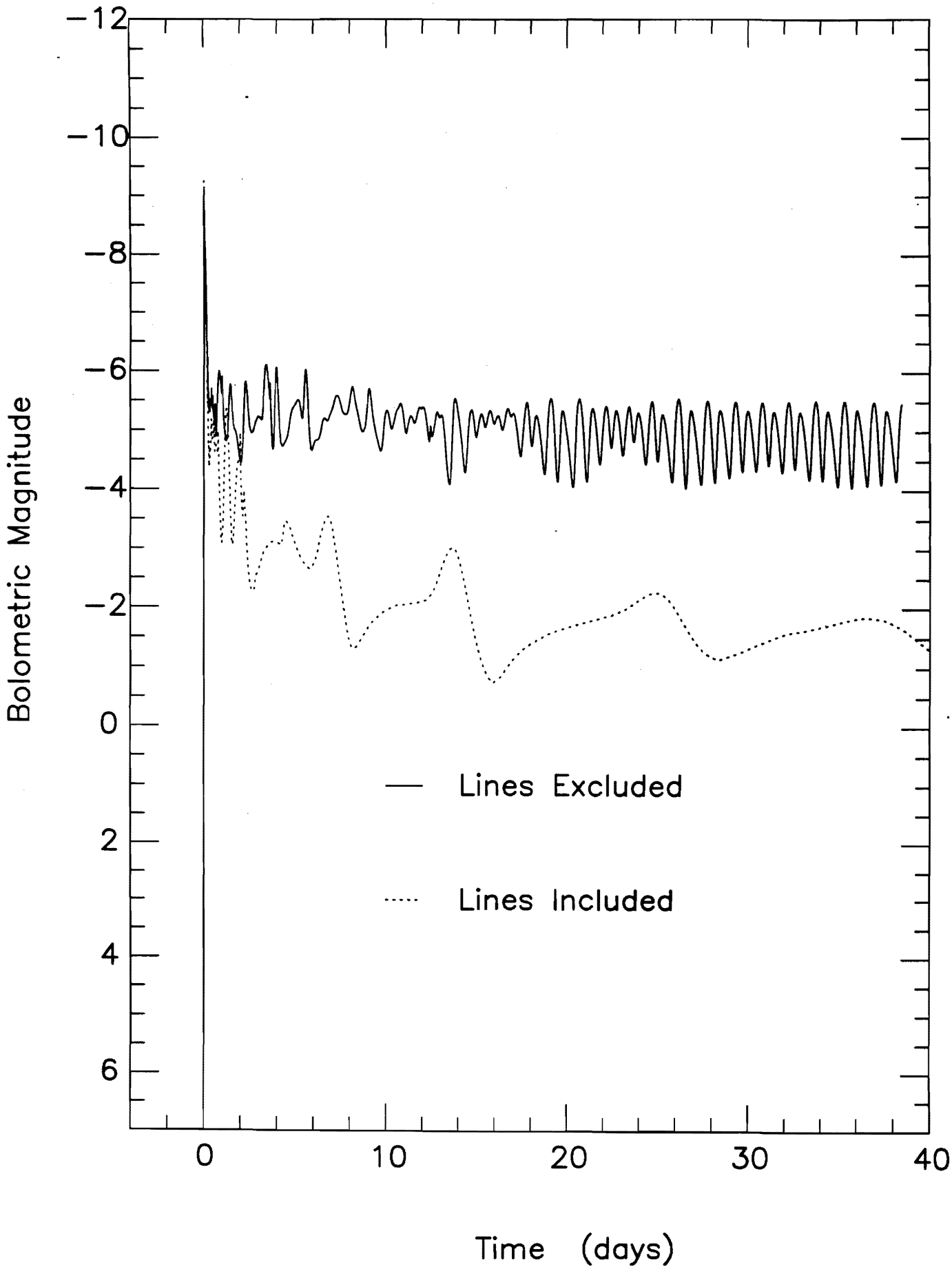
−12
−10
−8
−6
−4
−2
0
2
4
6
Bolometric Magnitude
0
10
20
30
40
Time (days)
Lines Excluded
Lines Included

FIGURE 2

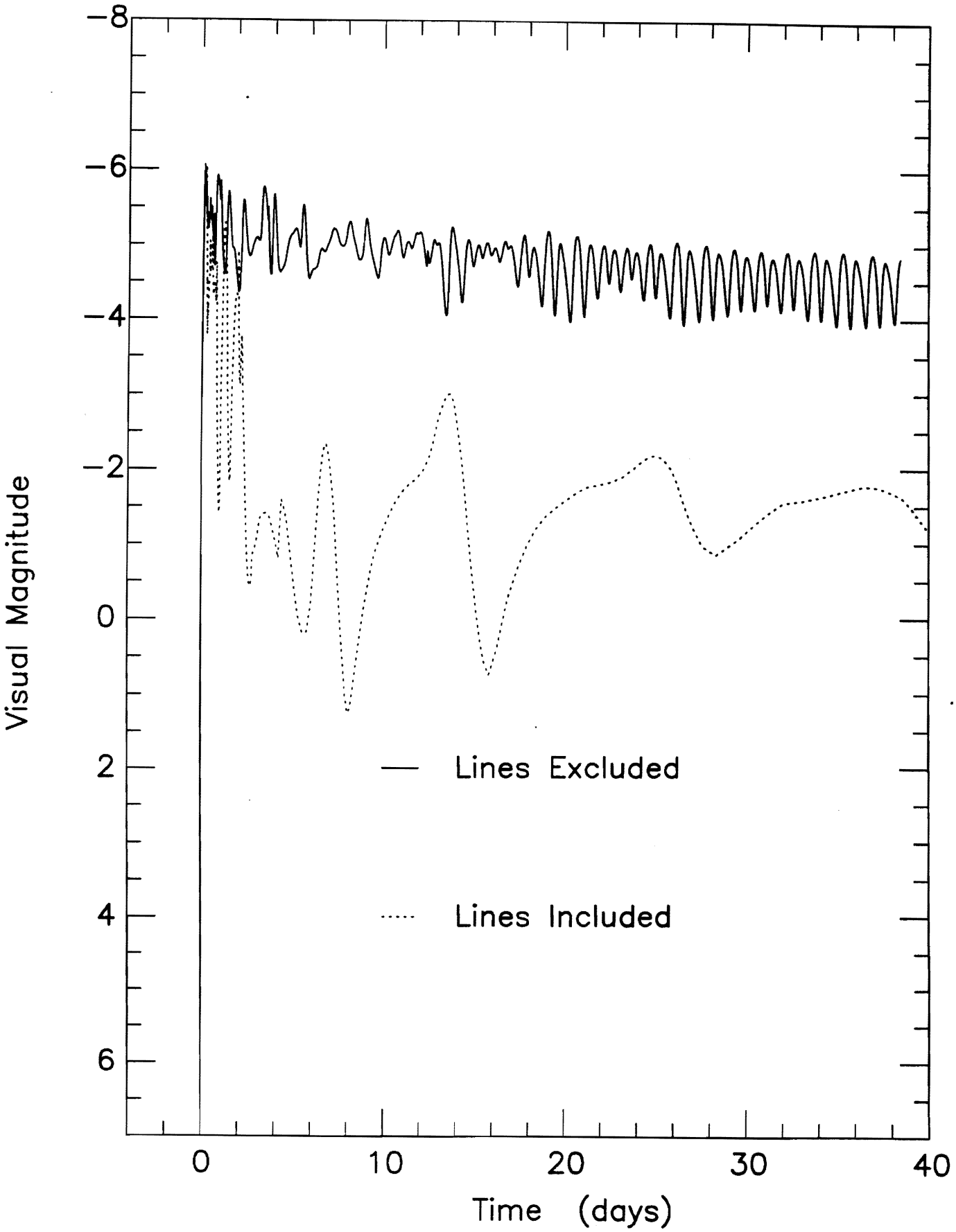
−8
−6
−4
−2
0
2
4
6
Visual Magnitude
0
10
20
30
40
Time (days)
Lines Excluded
Lines Included

FIGURE 3

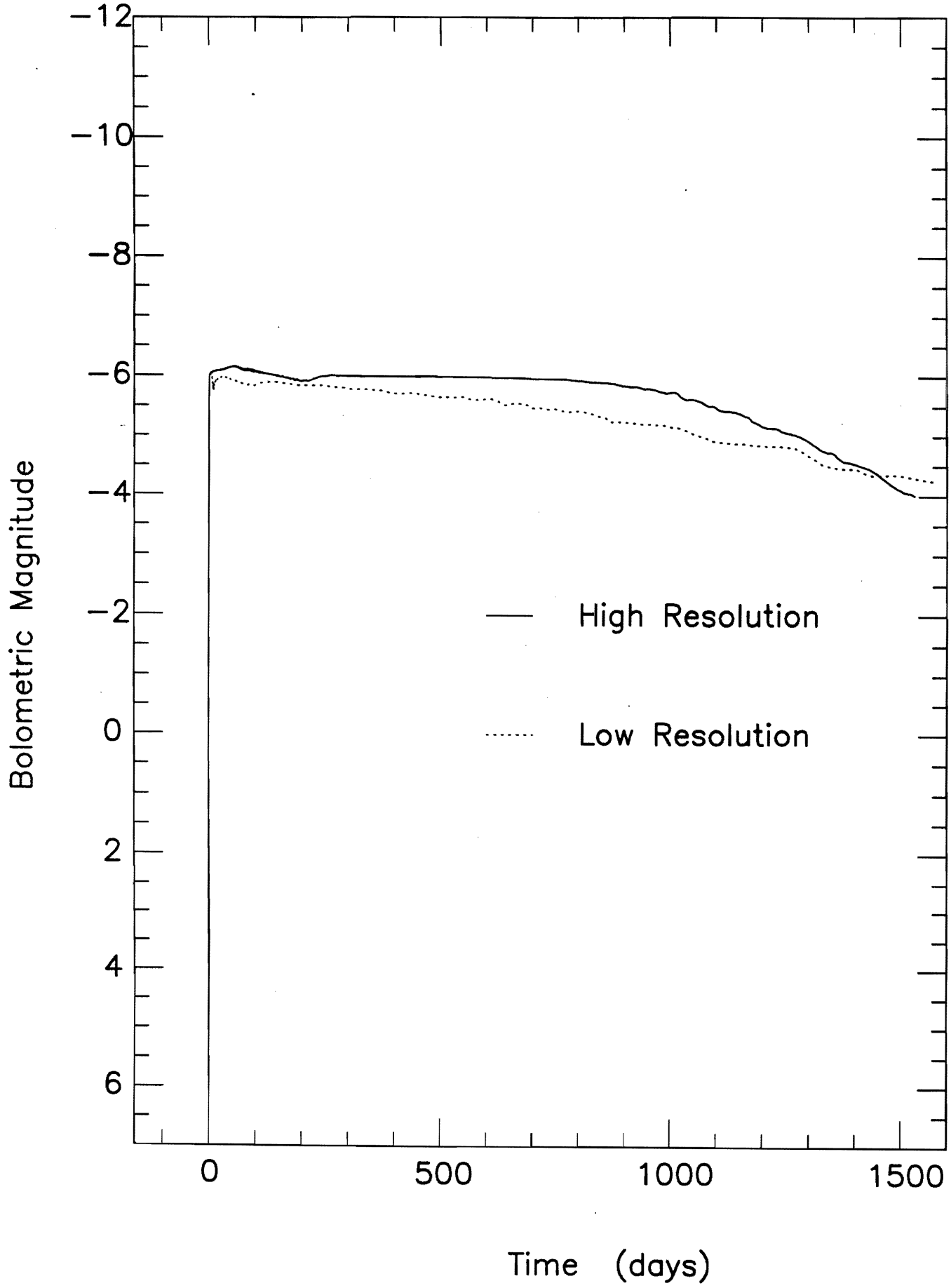
−12
−10
−8
−6
−4
−2
0
2
4
6
Bolometric Magnitude
High Resolution
Low Resolution
0
500
1000
1500
Time (days)

FIGURE 4

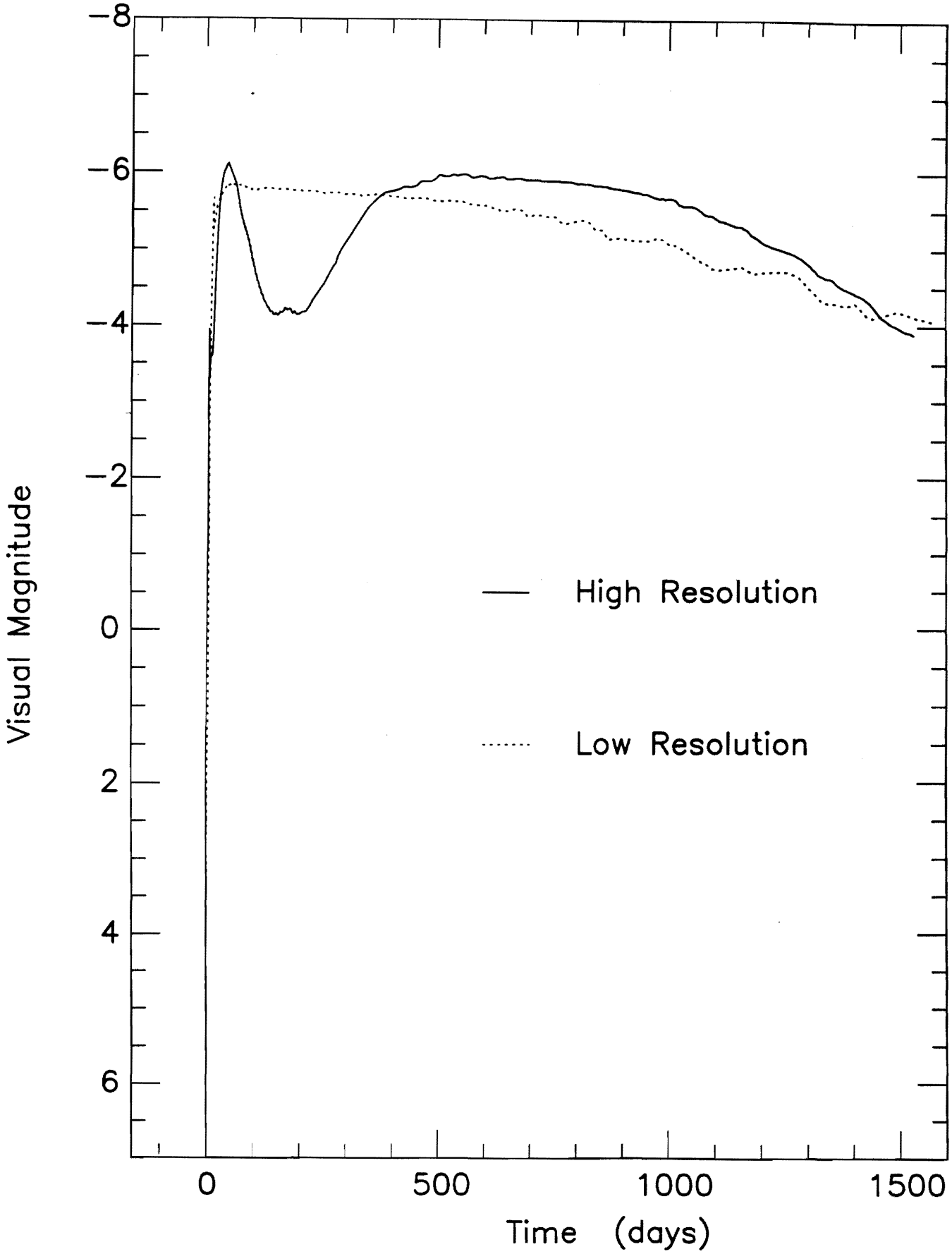
−8
−6
−4
−2
0
2
4
6
Visual Magnitude
High Resolution
Low Resolution
0
500
1000
1500
Time (days)

FIGURE 5

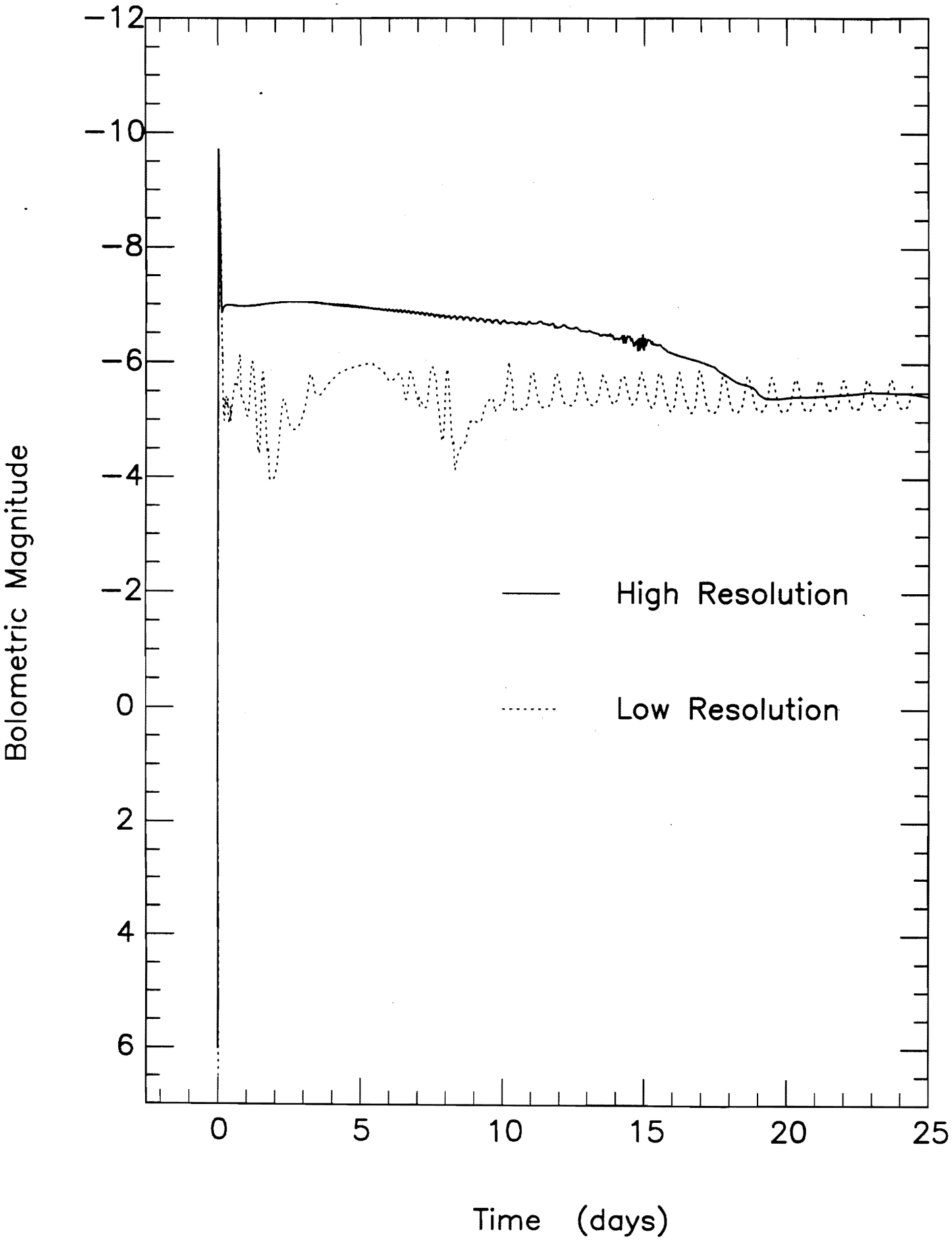
−12
−10
−8
−6
−4
−2
0
2
4
6
Bolometric Magnitude
High Resolution
Low Resolution
0
5
10
15
20
25
Time (days)

FIGURE 6

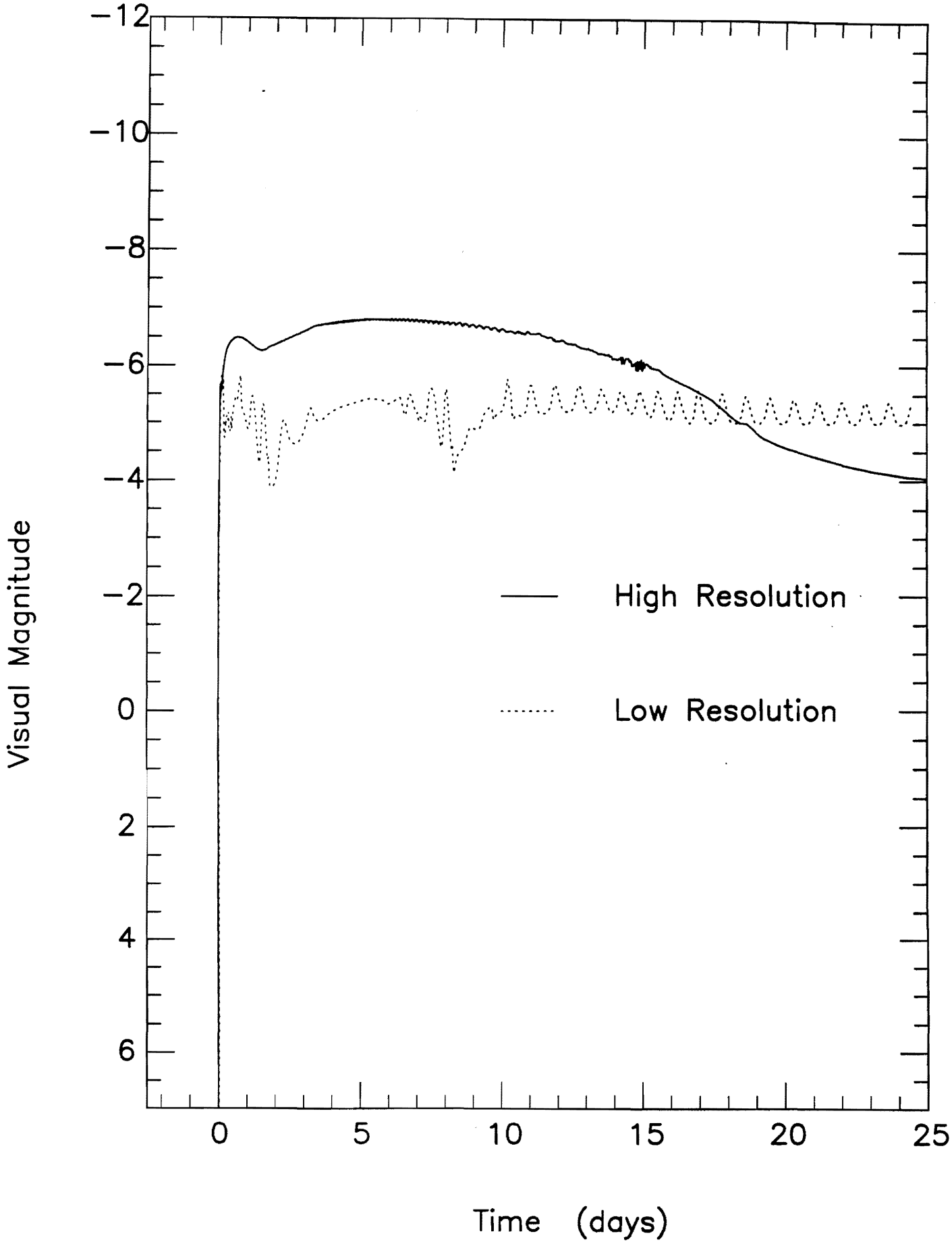
−12
−10
−8
−6
−4
−2
0
2
4
6
Visual Magnitude
0
5
10
15
20
25
Time (days)
High Resolution
Low Resolution

FIGURE 7

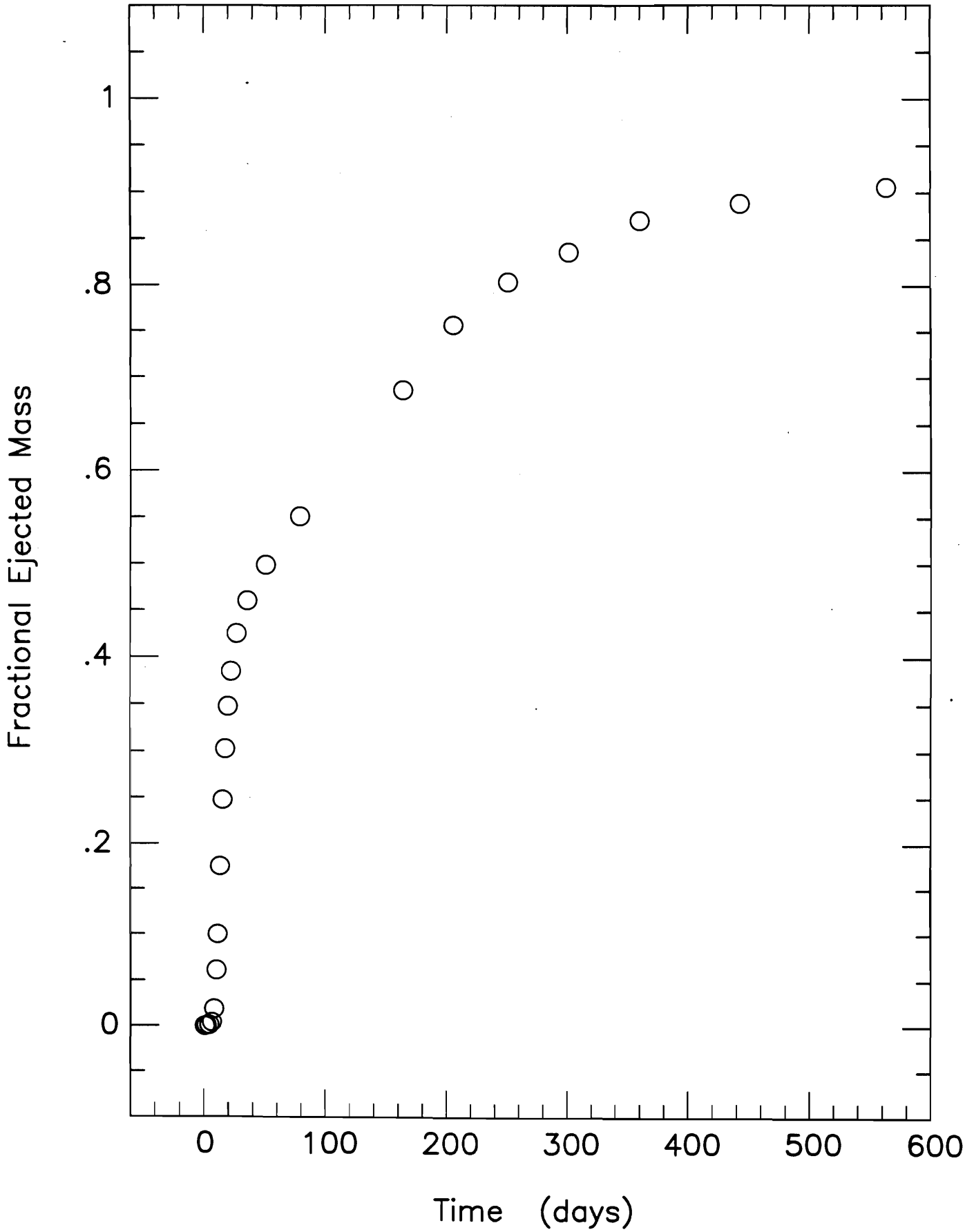
Fractional Ejected Mass
1
.8
.6
.4
.2
0
0
100
200
300
400
500
600
Time (days)

FIGURE 8

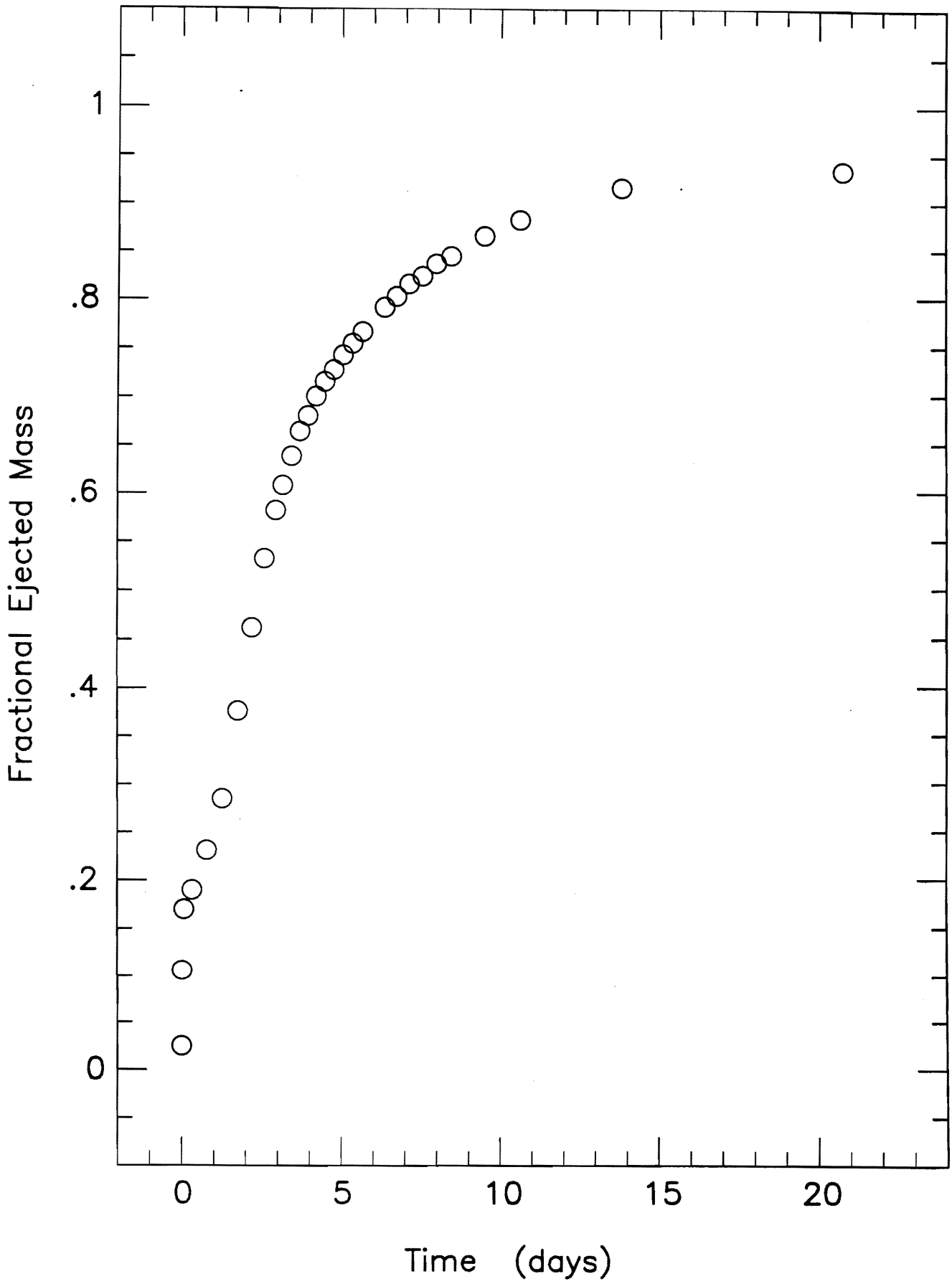

FIGURE 9

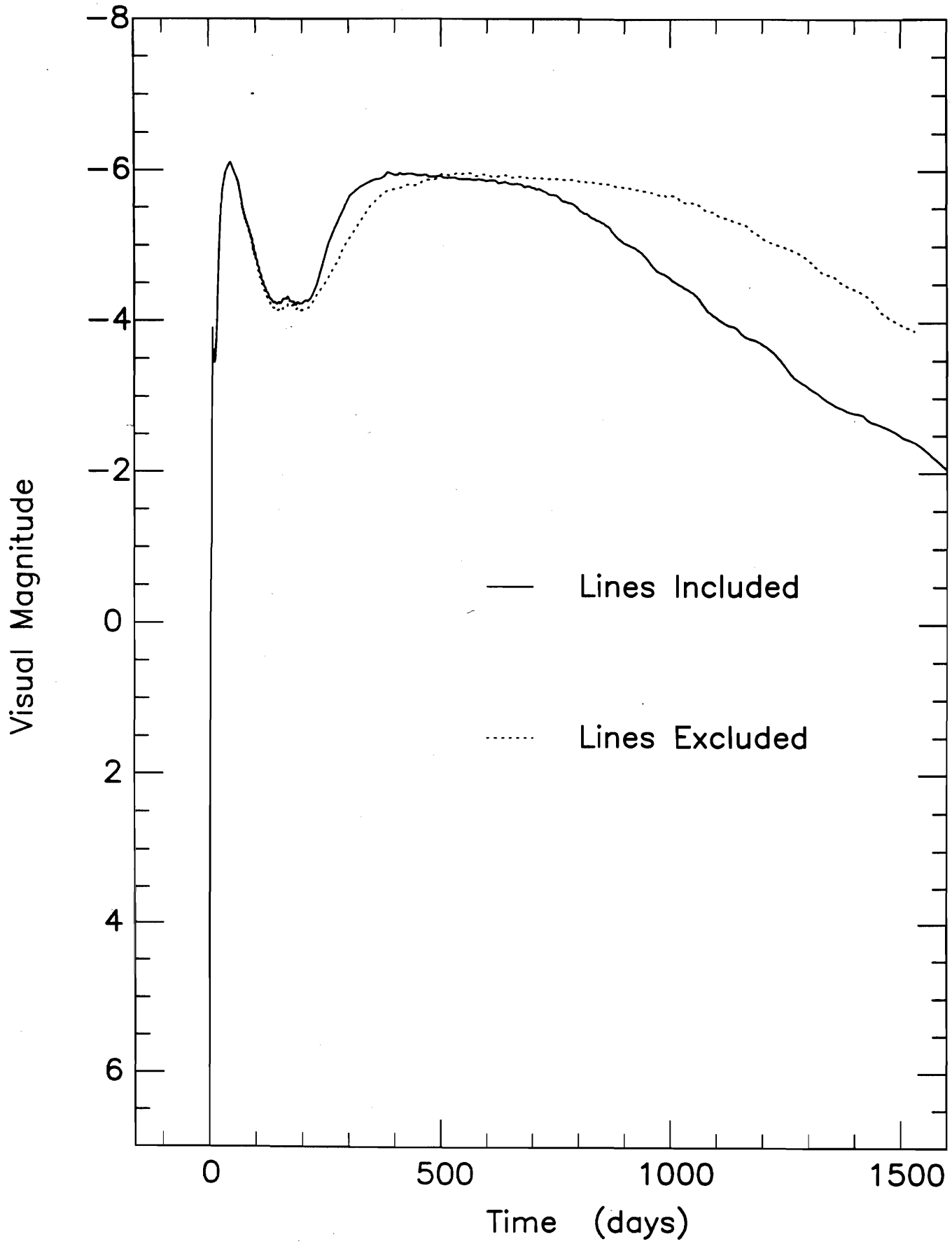
−8
−6
−4
−2
0
2
4
6
Visual Magnitude
0
500
1000
1500
Time (days)
Lines Included
Lines Excluded

FIGURE 10

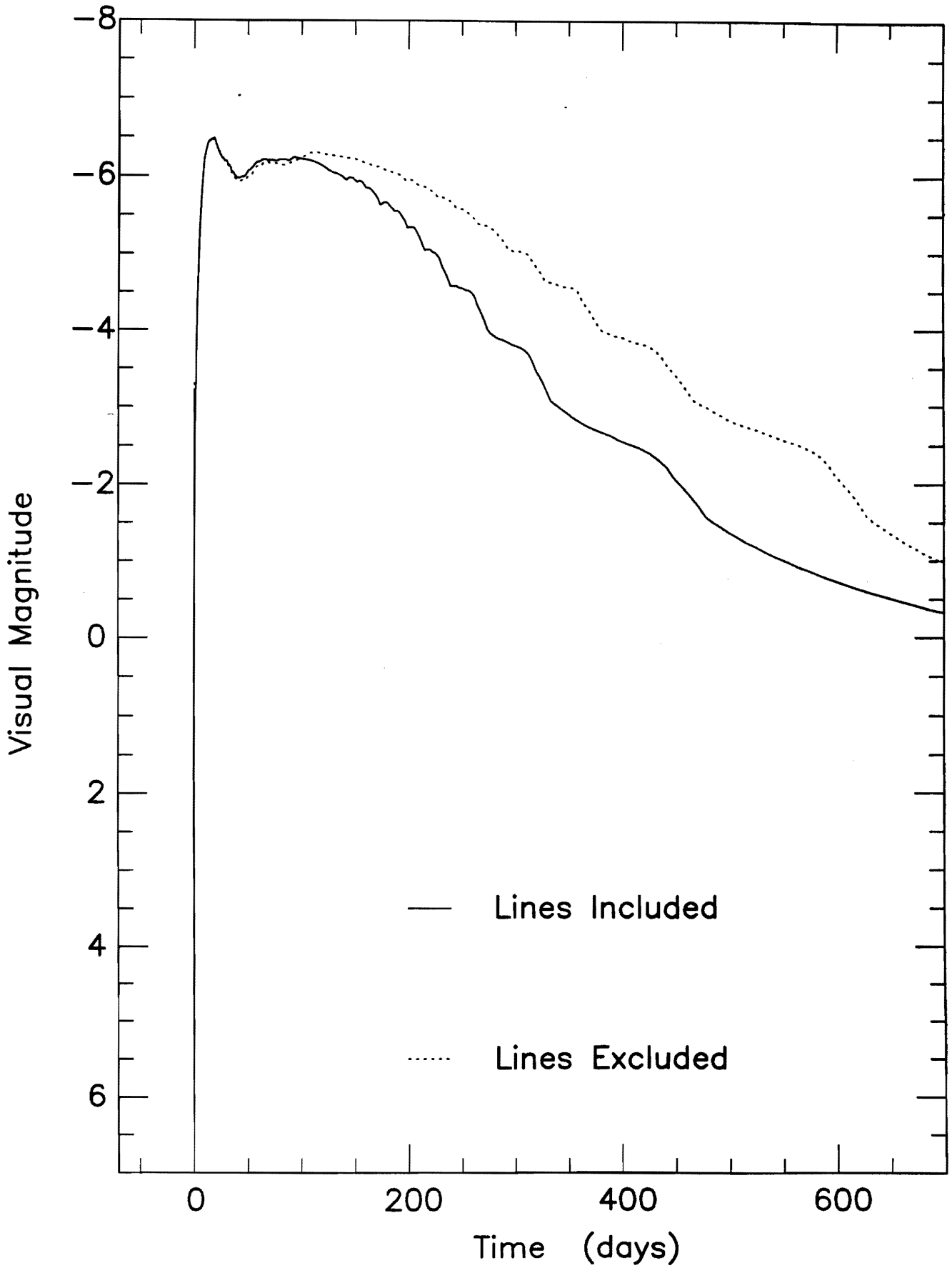
−8
−6
−4
−2
0
2
4
6
Visual Magnitude
0
200
400
600
Time (days)
Lines Included
Lines Excluded

FIGURE 11

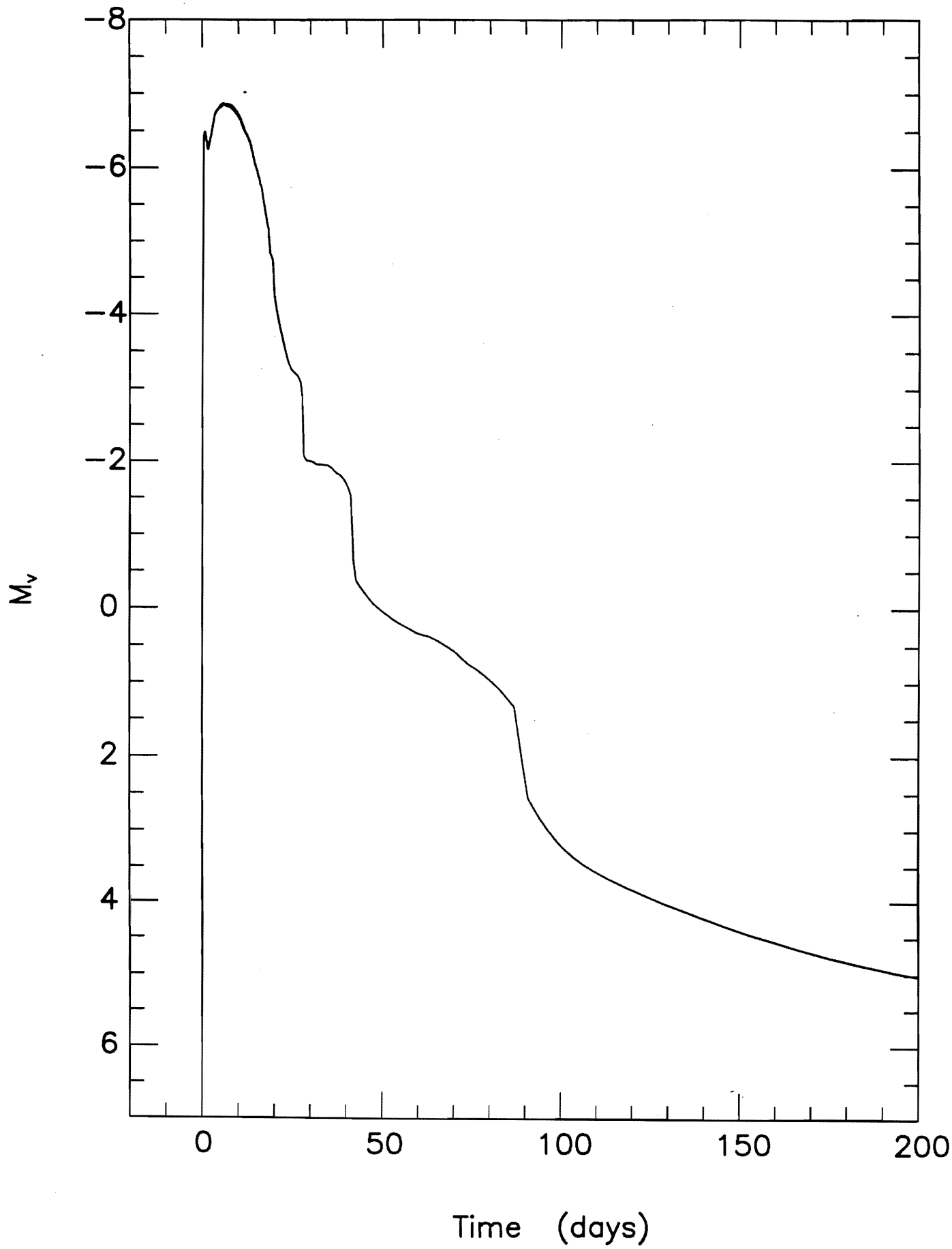

Table 1

Nuclear and wind depletion timescales, assuming accreted material of solar composition.

M_{wd} ($M_\odot$)	M_{env} ($M_\odot$)	τ_{nuc} (yr)	τ_{wind} (yr)
1.0	6.4×10^{-5}	168	10
1.25	2.1×10^{-5}	36	0.5
1.35	8.4×10^{-6}	20	7 days

Table 2

Nuclear and wind depletion timescales, assuming $Z_{cno} = 0.6$.

M_{wd} ($M_\odot$)	M_{env} ($M_\odot$)	τ_{nuc} (yr)	τ_{wind} (yr)
1.0	2.1×10^{-5}	55	3.4
1.25	7.6×10^{-6}	13	62 days
1.35	4.6×10^{-6}	11	4 days

Table 3

The maximum bolometric magnitude, for low- and high-resolution sequences.

	Sequence								
Quantity	1	2	3	4	5	6	7	8	9
$M_{wd}(M_\odot)$	1.00	1.00	1.00	1.25	1.25	1.25	1.35	1.35	1.35
Z_{cno} (by mass)	0.02	0.10	0.6	0.02	0.1	0.6	0.02	0.1	0.6
Max M_{bol} (l.r.)	-6.05	-6.06	-7.26	-6.53	-6.59	-9.57	-6.73	-7.00	-7.26
Max M_{bol} (h.r.)	-6.15	-6.20	-9.74	-6.56	-6.61	-9.72	-6.74	-7.06	-7.29

Table 4

The maximum visual magnitude, for low- and high-resolution sequences.

Quantity	Sequence 1	2	3	4	5	6	7	8	9
$M_{wd}(M_\odot)$	1.00	1.00	1.00	1.25	1.25	1.25	1.35	1.35	1.35
Z_{cno} (by mass)	0.02	0.10	0.6	0.02	0.1	0.6	0.02	0.1	0.6
Max M_{vis} (l.r.)	-5.83	-5.85	-5.86	-6.05	-5.96	-5.82	-5.57	-6.02	-5.61
Max M_{vis} (h.r.)	-6.11	-6.17	-6.49	-6.48	-6.48	-6.49	-6.60	-6.76	-6.60

Table 5

The maximum energy generation rate, for low- and high-resolution sequences 1 - 5.

Quantity	Sequence 1	2	3	4	5
$M_{wd}(M_\odot)$	1.00	1.00	1.00	1.25	1.25
Z_{cno} (by mass)	0.02	0.10	0.6	0.02	0.1
Max E_{nuc} (l.r.) (erg g^{-1} s^{-1})	8.9×10^{13}	1.1×10^{15}	5.7×10^{15}	1.1×10^{14}	5.7×10^{15}
Max E_{nuc} (h.r.) (erg g^{-1} s^{-1})	1.2×10^{14}	1.7×10^{15}	9.3×10^{15}	1.8×10^{14}	6.9×10^{15}

Table 6

The maximum energy generation rate, for low- and high-resolution sequences 6 - 9.

Quantity	Sequence 6	7	8	9
$M_{wd}(M_\odot)$	1.25	1.35	1.35	1.35
Z_{cno} (by mass)	0.6	0.02	0.1	0.6
Max E_{nuc} (l.r.) (erg g^{-1} s^{-1})	9.6×10^{16}	1.5×10^{14}	1.6×10^{16}	7.8×10^{16}
Max E_{nuc} (h.r.) (erg g^{-1} s^{-1})	1.2×10^{17}	1.3×10^{14}	2.2×10^{16}	1.0×10^{17}

Table 7

The fractional ejected mass, for low- and high-resolution sequences.

	Sequence								
Quantity	1	2	3	4	5	6	7	8	9
$M_{wd}(M_\odot)$	1.00	1.00	1.00	1.25	1.25	1.25	1.35	1.35	1.35
Z_{cno} (by mass)	0.02	0.10	0.6	0.02	0.1	0.6	0.02	0.1	0.6
M_{ej}/M_{env} (l.r.)	0.38	0.48	0.16	0.53	0.61	0.21	0.03	0.15	0.11
M_{ej}/M_{env} (h.r.)	0.88	0.88	0.79	0.91	0.94	0.96	0.93	0.85	0.73

Table 8

The fractional ejected mass, with and without line-driving effects; high resolution sequences only.

	Sequence					
Quantity	1	2	3	4	5	6
$M_{wd}(M_\odot)$	1.00	1.00	1.25	1.25	1.35	1.35
Z_{cno} (by mass)	0.02	0.6	0.02	0.6	0.02	0.6
M_{ej}/M_{env} (no lines)	0.88	0.79	0.91	0.96	0.93	0.73
M_{ej}/M_{env} (lines)	0.90	0.90	0.94	0.92	0.94	0.80